Global Journal of Science Frontier Research: a Physics and Space Science
Volume 25 Issue 5 Version 1.0 Year 2025
Type: Double Blind Peer Reviewed International Research Journal
Publisher: Global Journals
Online ISSN: 2249-4626 & Print ISSN: 0975-5896

Features of the Homogeneous Plasmonic Structures on Porous Silicon Formation

By K. B. Tynyshtykbayev
Kazakhstan Nazarbayev University

Abstract- In this work, we demonstrate the feasibility of fabricating uniform periodic plasmonic structure of Ni-PNP/por-Si by masking the wafer surface using optical lithography, followed by pore formation and deposition of plasmonic Ni-nanoparticles (Ni-PNP) in a single-step metal-assisted electrochemical etching process. It is shown that the high energetics of nc-PS and of the nc-PS/c-Si interface facilitates the formation of uniform plasmonic Ni-PNP/PS structures using a single-step pore etching and deposition of plasmonic nanoparticles.

GJSFR-A Classification: *LCC Code: QC176.8.N35*

Strictly as per the compliance and regulations of:

Features of the Homogeneous Plasmonic Structures on Porous Silicon Formation

K. B. Tynyshtykbayev

Abstracts- In this work, we demonstrate the feasibility of fabricating uniform periodic plasmonic structure of Ni-PNP/por-Si by masking the wafer surface using optical lithography, followed by pore formation and deposition of plasmonic Ni-nanoparticles (Ni-PNP) in a single-step metal-assisted electrochemical etching process. It is shown that the high energetics of nc-PS and of the nc-PS/c-Si interface facilitates the formation of uniform plasmonic Ni-PNP/PS structures using a single-step pore etching and deposition of plasmonic nanoparticles.

I. Introduction

The plasmonic properties of metal nanoparticles with a high density of free electrons, Me-PNP (Au, Ag, Cu, etc.), are of great interest in terms of increasing the efficiency of solar cells, photoelectrocatalytic hydrogen generators, and biosensors [1]. However, the catalytic activity of typical plasmonic metals (Au, Ag, Cu, Al) for H2 production is comparatively low [2]. Therefore, hybrid plasmonic nanostructures are created in which the plasmonic properties of Me-PNP are combined with additional improved catalytic properties of non-plasmonic metal catalysts (Pt, Ru, Rh, Ni), which in many cases are not present in single-component analogs. The hybrid plasmonic system exhibits increased catalytic activity due to a combination of efficient absorption of light by plasmonic nanoparticles and the transfer of concentrated energy to the charge carriers of the catalyst. In such systems, the decay of plasmonic resonances changes in favor of non-radiative heat generation, compared to radiative processes (scattering) [3]. Moreover, hybrid plasmonic structures exhibit increased chemical stability due to the formation of stable chemical bonds between the boundary atoms of the interface. Thus, enhanced light absorption due to the local field of Me-PNP and the increased injection rate of hot carriers from the plasmonics to the catalytic metal improves H2 production.

Enhanced light absorption by the interface and a corresponding shift in the spatial distribution of absorption toward the catalytic metal increases the lifetime of excited catalyst carriers, thereby increasing the efficiency of H2 and O2 evolution reactions [4].

Author: Physics and Technology Institute Satbayev University, Almaty 050032, Kazakhstan Nazarbayev University, Astana 010000, Kazakhstan. e-mails: k.tynyshtykbayev@sci.kz kurbangali.tynyshtykbayev@nu.edu.kz

Thus, the catalytic activity of plasmonic metals can be improved by combining plasmonic metals with conventional catalytically active metals, the inclusion of which can help reduce the activation energy of a reaction step or improve the dynamics of hydrogen generation on the catalyst surface. Combining the two metals reduces the chemical potential of charge carrier transfer across the interface and increases the efficiency of H2 and O2 gas separation reactions and their recovery [5]. The plasmonic properties of Ni-PNP nickel nanoparticles are weaker than those of plasmonic metals (Ag, Cu, Al) [6], as Ni-PNP exhibit stronger plasmon damping due to strong magnetic polarization [7], but they are less demanding to manufacture. The main advantage of Ni is its good catalytic properties in the hydrogen evolution reaction [8] and low cost.

To this end, we investigated the possibility of using Ni-NP nickel nanoparticles [7] to create a Ni-PNP/PS nickel plasmonic structure based on porous silicon (PS) as a supporting semiconductor core [9]. As is known [10], porous silicon nanocrystallites (nc-PS) are excellent catalysts for H2 evolution in water photoelectrolysis reactions.

PS with a periodically changing surface structure and possessing the properties of a diffraction grating [11] is attractive for the creation of a periodic structure due to its high porosity and the potential possibility of obtaining a plasmonic structure using a relatively simple electrochemical method of etching and deposition of a plasmonic-active metal - metal-stimulated etching [12]. In addition, nickel silicide NiSi, formed on the surface of PS (at the Ni-PNP/nc-PS interface), exhibits protective properties against corrosion in a wide range of pH 5-pH 11 [13].

Porous silicon, consisting of an ensemble of oxidized wide-bandgap (Eg = 1.8 - 2.9 eV) silicon nanocrystallites (nc-Si), occupies a special place in silicon technology, which still remains dominant in the electronics industry [14]. The high energy of porous silicon nanocrystallites nc Si/PS [15] determines the high catalytic activity of PS, which is twice as high as the catalytic activity of the Pt electrode in the hydrogen evolution reaction [16].

Porous silicon PS, containing nanoparticles of plasmonic metals Me-PNP, is, in essence, plasmonic nanostructures Me-PNP/PS, localizing the scattering and absorption of light near The free-electron oscillation frequencies of Me-PNPs are sources of localized

plasmonic resonance radiation. The porous PS structure is used as a supporting framework for plasmonic PNP nanoparticles. By controlling the morphology, shape, and size of the pores, as well as the conductivity type of the silicon framework in the form of p-type silicon for the photocathode, the PS structure can be tailored for efficient photocatalysis of a specific hydrogen evolution reaction at the cathode, making them promising systems for achieving high hydrogen production selectivity. The developed PS surface allows for the concentration of plasmon-activated catalytic centers on the electrode surface near the region of plasmon resonance enhancement, increasing the efficiency of the H2 evolution reaction in the pores near the plasmonic Me-PNPs.

Furthermore, during the formation of the Ni-PNP/PS nickel plasmonic nanostructure, chemically stable silicide coatings form on the pore surface, increasing the stability of such structures in H2 evolution reactions [16].

The main drawback of plasmonic structures based on Me-PNP/PS porous silicon is the lack of periodicity in the arrangement of pores or nanocrystallites of porous silicon, nc-Si/PS. We have demonstrated the feasibility of creating a strictly periodic Ni-PNP/PS nickel plasmonic structure by masking the surface of a c-Si single crystal using optical lithography and subsequent pore formation in a single-step metal-assisted electrochemical etching process.

This paper presents the results of the fabrication of uniform periodic plasmonic Me-PNPs/por-Si structures by masking the wafer surface using optical lithography, and followed by the formation of pores and the deposition of plasmonic-active metal nanoparticles (Me-PNPs) in a single-step metal-assisted electrochemical etching (MACE) process. The photoluminescence properties of the nickel plasmonic Ni-PNP/PS structure formed on the basis of the Ni+ ion-implanted textured surface (SiO2/c-Si) of silicon wafers by the deposition of nickel nanoparticle (Ni-NPs) in a single-step process of the formation of the periodic porous silicon (PS) structure and the deposition of Ni-NP nanoparticles by the combined EMACE method—a combination of electrochemical (EC) and MACE of single-crystal silicon c-Si—are also investigated.

II. Experimental Procedure (Method)

In this work, we used p-Si (100) single crystal wafers, 10 ohm cm, with a diameter of 100 mm and a thickness 500 mkm of grown by the Czochralski method. The samples were preliminarily thermally oxidized at 1000°C in an oxygen atmosphere for 100 min to form a 500 nm thick layer of thermal silicon oxide (SiO_2 therm.) on the surface. A checkerboard texture with alternating areas 100 × 100 μm2 of thermal SiO2 and crystalline c-Si (SiO2 therm./c-Si) was created on the oxidized silicon surface by using optical lithography for masking and opening the oxide layer, Fig. 1. The SiO2 layer was used as a protective window during etching of pores in c-Si and as an optical window of the silicon photoelectrode, transparent to sunlight, during photoelectrolysis of water [8].

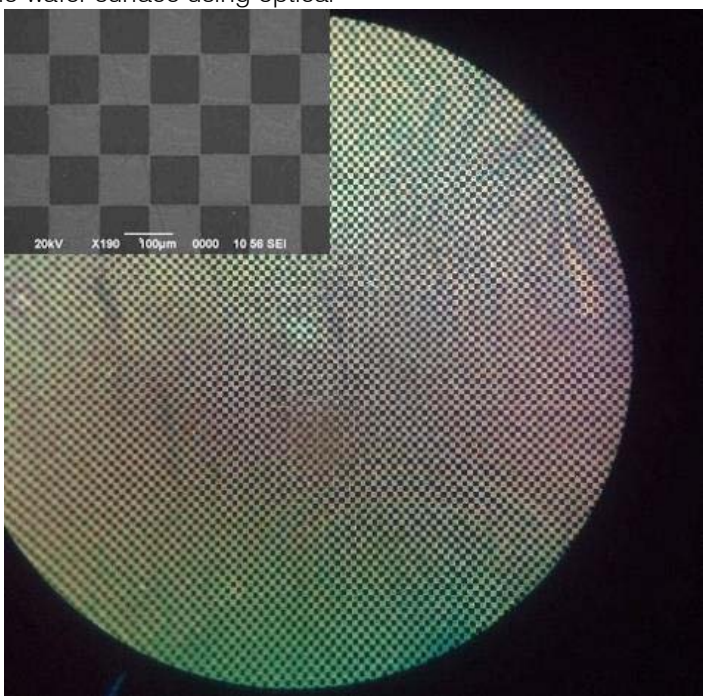

Fig. 1: Photograph of a textured silicon wafer surface with alternating areas of pure c-Si and thermal SiO2. Inset: SEM image of a textured surface area of c-Si and SiO2 thermal; 001 –SiO2 thermal, 002 – c-Si. The technique for creating alternating SiO2 thermal windows is described in detail in [16].

To form an ohmic contact, a 300 nm thick aluminum layer was deposited on the back side of the wafer using magnetron sputtering, and followed by annealing at 400°C for 30 min under a vacuum of $5 \cdot 10^{-5}$ Torr.

Pores on the textured c-Si/SiO2 thermical surface were formed by electrochemical etching (EC) in weak (8% HF: 3% H_2O_2 - E1) and strong (55% HF: 40% H2O2 - E2) hydrogen fluoride electrolytes. Weak electrolyte E1 was used to form pores in exposed areas of crystalline c-Si while preserving areas with the SiO2thermical oxide layer. Strong electrolyte E2 dissolved the SiO2 thermical silicon oxide and formed pores over the entire surface of the textured silicon wafer. The Ni-PNP/PS nickel plasmonic structure was formed by etching the textured c-Si/SiO2 surface of the silicon wafer implanted with 100 keV Ni+ ions at a dose of 10^{16} cm^{-2}. Ni+ ions were implanted in exposed areas of c-Si crystalline silicon, free from the protective SiO2 thermal oxide layer. The introduction of Ni+ ions is shown schematically in Fig. 2.

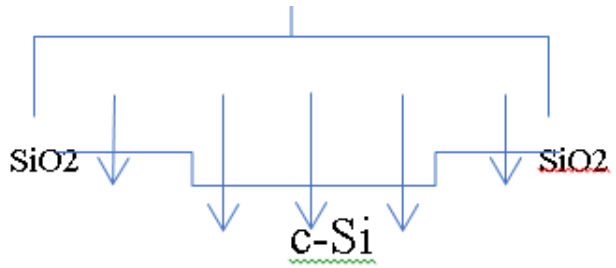

Fig. 2: Schematic diagram of Ni+ ion implantation in c-Si.

The implantation depth of Ni+ ions with an energy of E = 100 keV was approximately 60 nm, see Fig. 3.

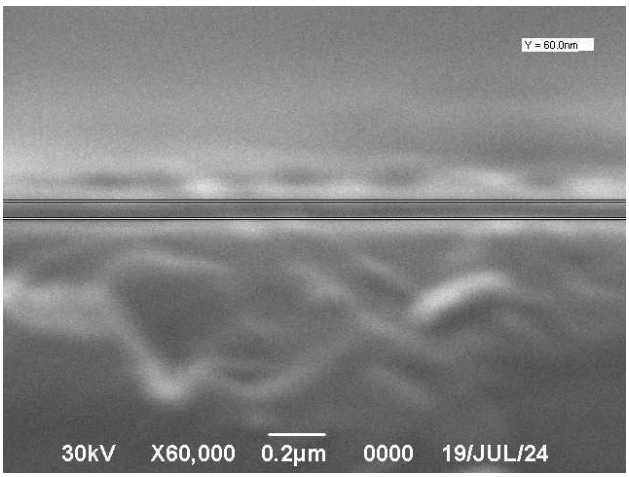

Fig. 3: SEM image of a cross-section of c-Si implanted with 100 keV Ni+ ions.

Samples were analyzed using a Carl Zeiss Auriga Crossbeam 540 Scanning Electron Microscope with an X-ray Energy-Dispersion Analyzer, a Raman spectrometer, the Horiba LabRam Evolution, a UNICO Spectro Quest 2800 spectrophotometer, and a DRON-4 X-ray diffractometer.

III. Results and Discussion

Figure 4 shows SEM images of a textured silicon wafer surface with alternating areas of porous silicon and silicon dioxide SiO2, obtained by EC etching in E1 electrolyte.

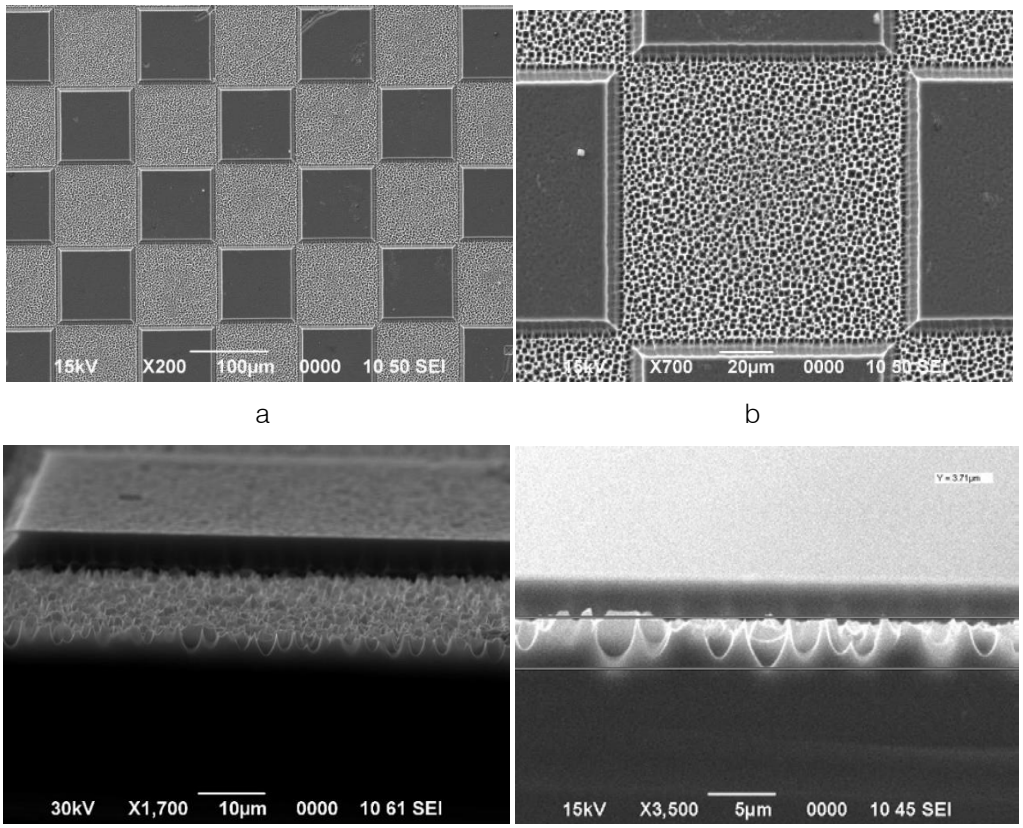

Fig. 4: SEM images of a textured silicon wafer surface with areas of PS and SiO2 (a)–(c) and a transverse cleavage (d).

It is evident that uniform pores of virtually identical sizes form in the exposed areas of crystalline c-Si silicon; the pore diameters are commensurate with their depth (Fig. 4d). This is achieved due to the action of long-range elastic-deformational stress forces arising at the c Si/SiO2 interface due to differences in their structures [15], which causes the formation of uniform pores in the near-boundary region. As these forces weaken, non-uniform pores form, Fig. 5. Thus, the action of elastic-deformational forces at the c-Si/SiO2 interface boundaries leads to the formation of uniform pores.

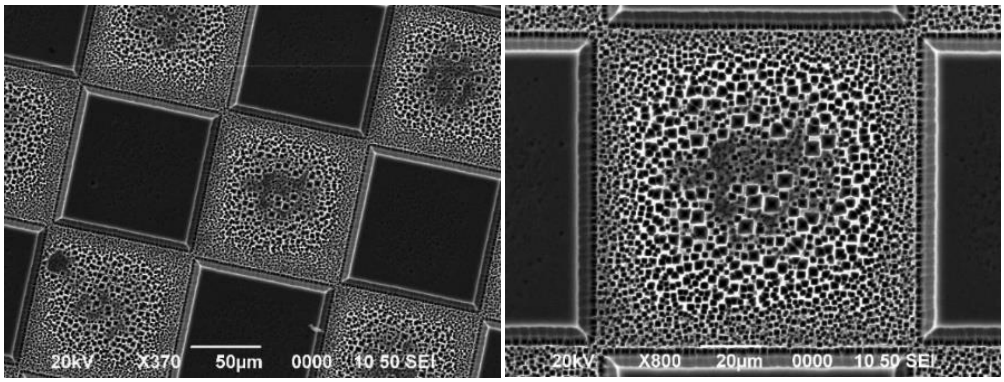

Figure 5: SEM image of the porosity distribution of the PS region with increasing distance from the interface boundaries.

Thus, creating alternating c-Si/SiO2 interface boundaries by pre-masking the silicon wafer surface using optical lithography allows for the formation of uniform pores. This will overcome the main drawback of porous silicon for formation of the Me-PNP/PS plasmonic nanostructure— the lack of periodicity in the arrangement of pores or nanocrystallites of porous silicon, nc-Si/PS and to create of periodic plasmonic structures on porous silicon by depositing plasmonic metal nanoparticles on them.

On the SEM- image of the nickel plasmonic structure Ni-PNP/PS clearly shows nickel containing areas and areas of pure porous silicon without nickel, Fig. 7a. Area 001 does not contain Ni lines in the EDS (Fig. 7b) and corresponds to purely porous silicon PS, and the ED spectrum of area 002 shows the presence of Ni peaks (Fig.7c), which indicates porous silicon with nickel content, PS<Ni>. This is also confirmed by brightness of the SEM images of region 002, which is bright, than the region 001, because the intensity of secondary reflected electrons increases with increasing average atomic number [17]; it is higher for Ni (59) than for I (28). Therefore, region 002, containing PS<Ni>, has a higher brightness than the pure PS layer without Ni, region 001.

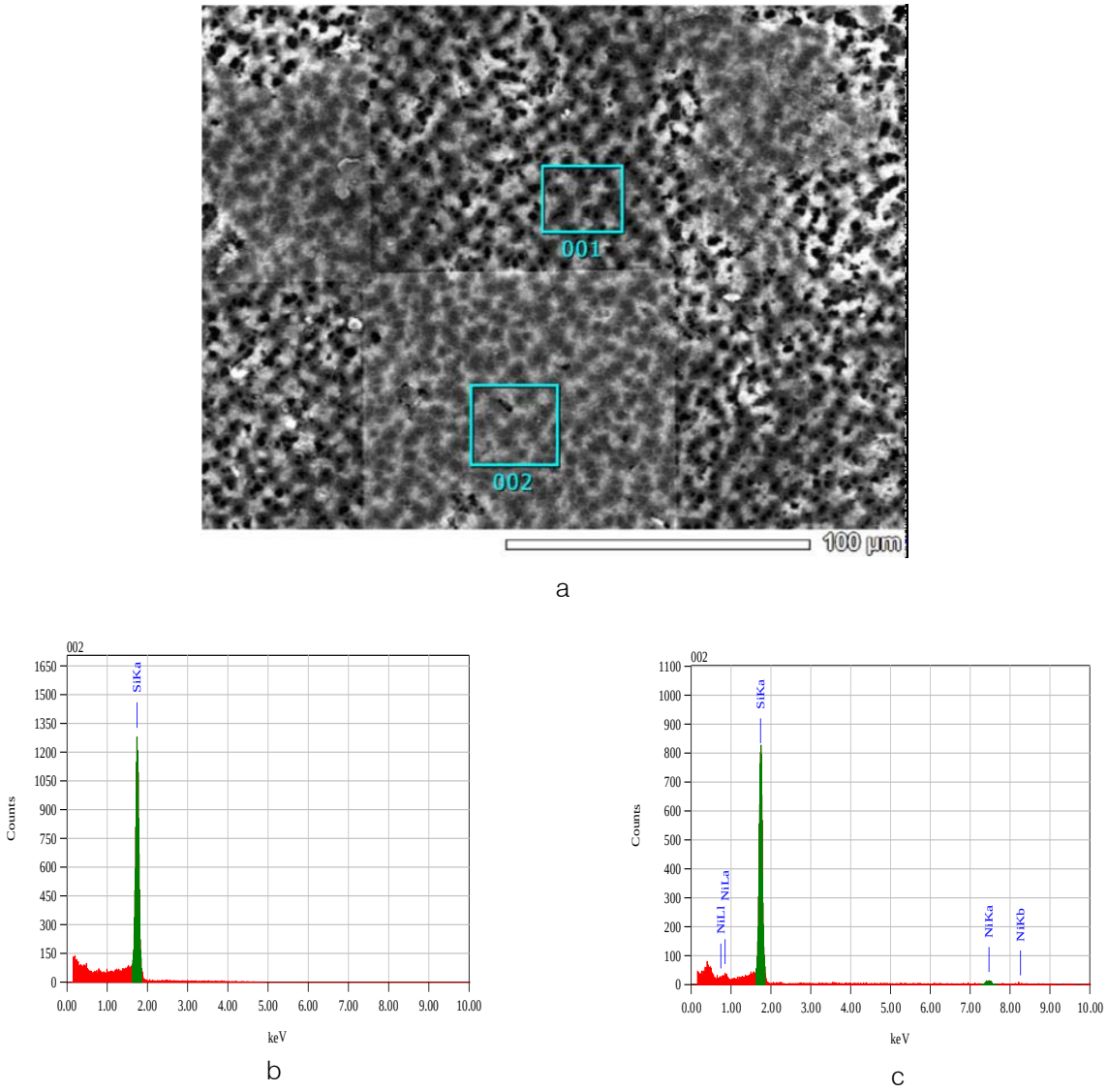

Figure 6: SEM image of Ni-PNP/PS sample (a) and EDS of regions 001 (b) and 002 (c).

It should be especially noted that in Figure 6a, in region 002, a rectangular region is clearly observed, which appeared due to the silicide layer formed during thermal annealing of the contacts at 400◦C. The X-ray spectrum of this sample (Figure 7) shows the presence of NiSi lines, characteristic of nickel silicides [16].

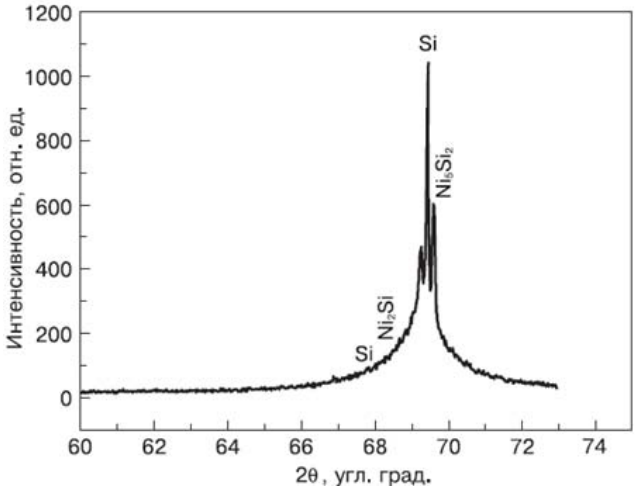

Fig. 7: X-ray diffraction spectrum of a silicide coating [16].

This silicide layer is characterized by high chemical stability [16].

Figure 8 shows optical image (a) and PL spectra (b) of a sample with a Ni-PNP/PS structure. It can be seen that the central region containing the Ni-PNP/PS is orange, unlike the edge, where the plasmonic structure did not form, and is characterized by stronger PL than the unetched region.

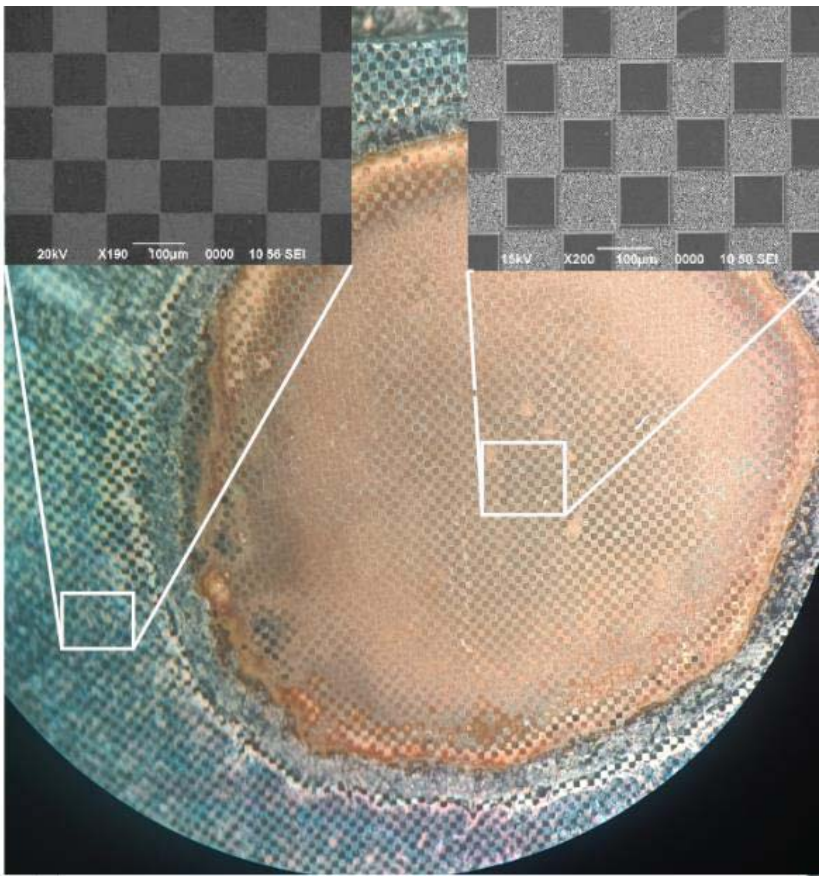

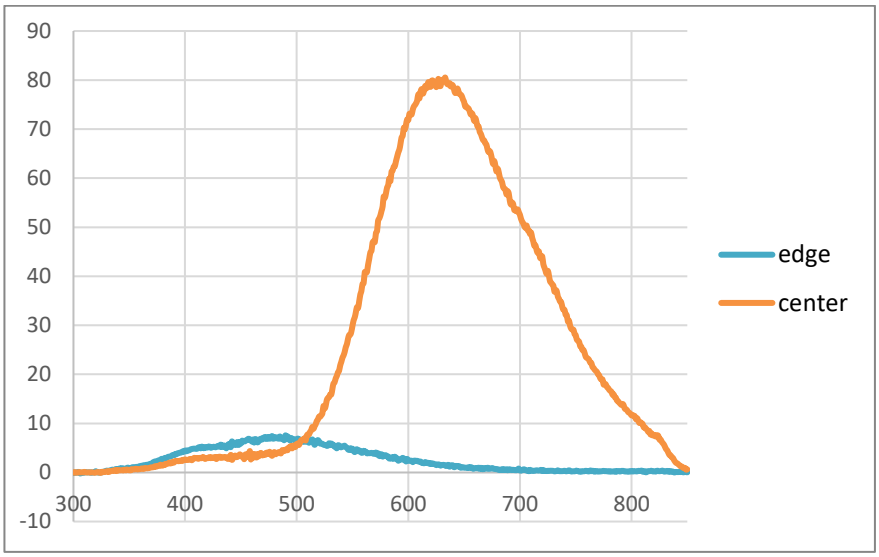

Figure 8: Photograph of a Ni-PNP/PS sample with a structure (a); PL spectra: - the etched porous region is shown in red; the unetched region is shown in blue.

When illuminated with a red LED, the porous region exhibits a brighter luminescence (Fig. 9a) than the unetched region (Fig. 9b).

a b

Fig. 9: Photograph of the luminosity of the etched and unetched original sample region illuminated by a red LED.

To analyze the luminosity, we recorded reflectance spectra in the 200–1100 nm wavelength range, Fig. 10.

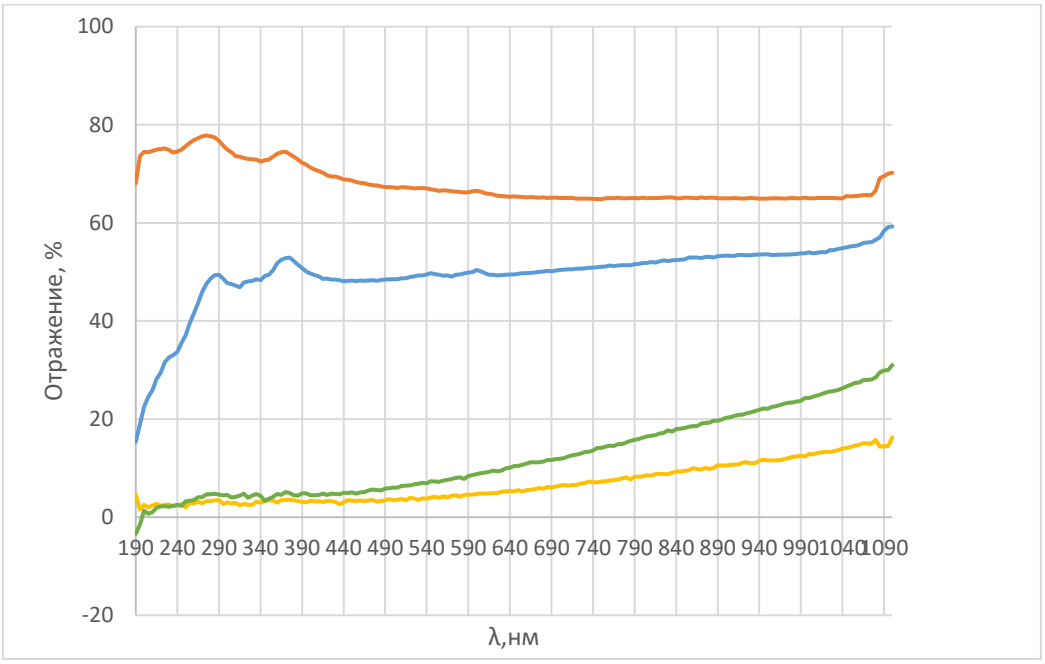

Fig. 10: Reflectance spectra of the original silicon substrate (brown), porous silicon in electrolyte E1 (blue), porous silicon in E2 (green), and plasmonic structure (yellow).

The reflectance spectra of these samples show that the reflection of light with an intensity of … in the wavelength range of 200 – 1100 nm for the matte surface of the original silicon substrate is at the level of 70%, for porous silicon from 10% to 50% depending on the porosity, and for the plasmonic structure 2-3% in the UV region, 5-7% in the visible region (400 – 700) nm and up to 15% for long wavelengths > 800 nm.

That is, the reflectance spectra indicate that the luminosity is due not to the reflectivity of the surface of the samples, but to the radiative properties of the plasmonic structure of Ni-PNP/por Si.

As is known [18], the nature of the enhancement of the optical signal of photoluminescence and Raman scattering of light by plasmonic structures is due to the resonant excitation of plasmons, Free electron vibrations in metal nanoparticles, the intensity of which depends on the morphology of the nanostructures, the electron density of the plasmonic nanoparticles, and the dielectric environment. Figure 11 shows the Raman spectra for crystalline (c-Si) and porous silicon with and without nickel, prepared by different methods.

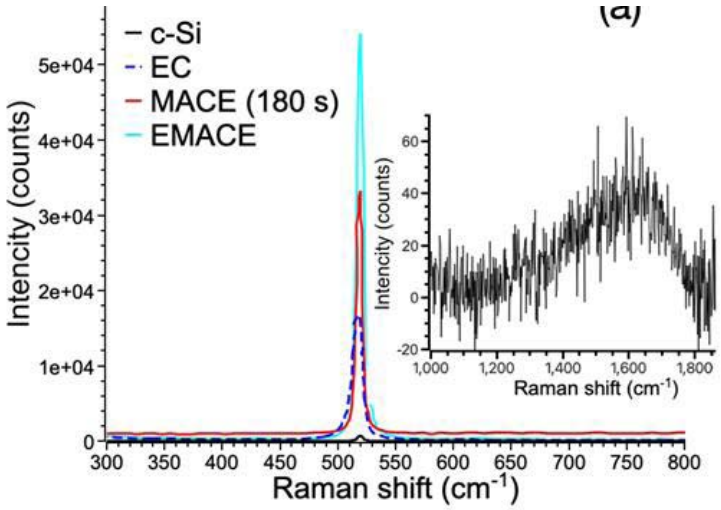

Figure 11: Raman spectra of porous silicon prepared by different methods. The Raman signals from regions associated with carbon bonds for samples prepared by the EMACE method are shown in the inset (a).

The highest intensity of the Raman peak Ipor-Si(EMACE) = 54,000 rel. units is observed for the por-Si(EMACE) sample at a Raman shift frequency of ν = 520.32 cm-1, formed by the combined method (MACE + EC). The high intensity of the Raman peak indicates a higher pore density and an increase in the concentration of scattering centers [19].

The Raman spectra also show that samples with higher porosity have a higher Raman peak intensity at a high frequency shift, as shown in Fig. 5a. The highest Raman peak intensity Iν = 54,000 counts at a frequency of 520.32 cm-1 is observed for the sample fabricated by the EMACE method. For the MACE sample, the intensity and frequency values are 33,000 counts and 519.66 cm-1, respectively. The sample fabricated by the EC method exhibits values of 17,000 counts at 519.11 cm-1. The Raman peak intensity for c-Si is 2,000, and the corresponding frequency is 519.11 cm-1. The Raman spectra of c-Si and PS exhibit a characteristic resonance peak due to electron-phonon scattering, the intensity and frequency of which depend on the concentration of scattering centers and, consequently, on the pore formation conditions. The high-frequency shift and the decrease in the full width at half maximum (FWHM) of the main peak due to the increase in the peak intensity are most significant in the sample fabricated by EMACE. This phenomenon is attributed to the increase in the number of Raman centers in nanocrystalline silicon [18]. Since the samples fabricated by EC and EMACE exhibit similar levels of porosity (Fig. 11), the enhancement of the Raman signal cannot be attributed solely to the increase in porosity. Even a small amount of metal content can be crucial in enhancing the Raman peak intensity. Note that the Raman spectra for all samples show no Ni-related nanoscale features at 550 cm-1 [20]. A possible additional source of Raman peak enhancement is the doping of substitutional (NiSi) and interstitial (NiI) nickel atoms incorporated into the silicon matrix. Since the high rate of nickel absorption into silicon has been previously documented in numerous experiments [21], we simulated substitutional (NiSi) and interstitial (NiI) defects [22]. The simulation details are the same as in our recent work [23]. As shown in Figs. 12a and 12b, the electronic structure of the substitutional nickel impurity exhibits the same peak at the Fermi level as silver (see Fig. 12c). Since silver nanostructures exhibit Raman peak enhancement, we can attribute the increase in Raman peak intensity in the EMACE-prepared sample to changes similar to those of silver in the local electronic structures of the Ni-doped silicon matrix.

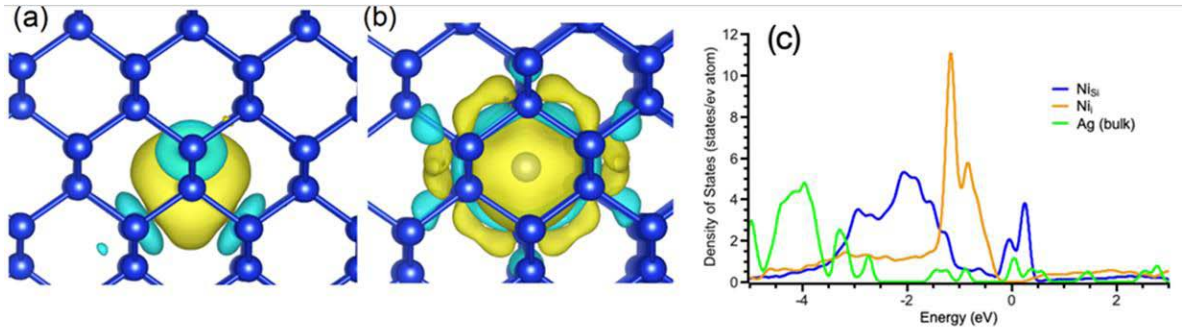

Figure 12: Changes in charge density after incorporation of substituent (a) and interstitial (b) nickel impurities. Yellow "clouds" correspond to an increase in charge density, while blue "clouds" correspond to a decrease in charge densities. Panel (sc) depicts the partial densities of states for metallic silver, substituent, and interstitial nickel impurities in the silicon matrix

To verify the possibility of carbon nucleation, described for cz-Si [24], and the formation of some ordered carbon structures, Raman spectra were obtained in the range from 1000 to 2000 cm-1 in the sample with the highest carbon content (EMACE). The results of the measurements demonstrate the presence of some carbon-carbon bonds in the spectra (see inset in Fig. 11a) without the distinct D and G peaks typical of layered carbon structures [25]. Based on the low Raman signal from these carbon structures and the absence of peaks corresponding to an ordered carbon structure, we can conclude that these carbon structures do not affect the enhancement of the Raman signal.

Moreover, the Raman peak intensity of the sample prepared by EMACE is almost twice that of the samples prepared by EC (33,000 counts versus 17,000 counts) [19].

Thus, preliminary masking of the silicon wafer surface allows for the formation of uniform pores. This avoids the main drawback of porous silicon as the backbone of the Me-PNP/PS plasmonic nanostructure—the lack of periodicity in the arrangement of pores or nanocrystallites of porous silicon, nc-Si/PS.

This allows the creation of periodic plasmonic Ni-PNP/PS structures using single-step EMACE

etching, which involves masking the surface of a single-crystal silicon with a photomask and then forming pores by etching c-Si.

IV. Main Results and Conclusions

Pre-masking the surface of silicon wafers with a photomask and subsequent single-step etching in a nickel-containing hydrofluoric acid electrolyte solution using the EMACE method enables the production of periodic nickel plasmonic Ni-PNP/PS structures with plasmonic properties. Ni-PNP/PS porous silicon-based plasmonic structures exhibit enhanced Raman and photoluminescence signals.

DFT simulation results showed that even small amounts of metal content can be crucial in increasing Raman peak intensity.

Acknowledgements

The work was supported by the Ministry of Science and Higher Education of the Republic of Kazakhstan, project BR21881954 "Development of technologies for the synthesis of nanostructured materials for the creation of effective photocatalytic electrodes, photo- and gas sensitive sensors". The author acknowledges Arman Yeltay (Universidade de Brasilia), Mansur Ydyrys (Nazarbayev Intellectual School), and PhD Ardak Ainabayev (Nazarbaev University) for their assistance in the paper preparation.

References Références Referencias

1. S. Ezendam, M. Herran, L. Nan, C. Gruber, Y. Kang, F. Gröbmeyer, R. Lin, J. Gargiulo, A. Sousa-Castillo, and E. Cortés. ACS Energy Lett. , 7, 778 (2022).
2. S. Lee, H. Hwang, W. Lee, D. Schebarchov, Y. Wy, J. Grand, B. Auguie, D.H. Wi, E. Cortes, S.W. Han. ACS Energy Letters. , 5 , 3881 (2020).
3. K. Li, N.J. Hogan, M.J. Kale, N.J. Halas, P. Nordlander, P. Christopher. Nano Lett. , 17, 3710 (2017).
4. C. Engelbrekt, K.T. Crampton, D.A. Fishman, M. Law, V.A. Apkarian. ACS Nano. , 14, 5061 (2020).
5. P. Peljo, J.A. Manzanares, H.H. Girault. Langmuir. , 32, 5765 (2016).
6. M.M. Abouelela, G. Kawamura, and A. Matsuda. J. Cleaner Production. , 294, 126200 (2021).
7. J. Chen, P. Albella, Z Pirzadeh, P Alonso-González, F. Huth, S. Bonetti, V. Bonanni, J. Åkerman, J. Nogués, P. Vavassori, A. Dmitriev, J. Aizpurua, and R. Hillenbrand. Small. , 7, 2341 (2011).
8. S. Hu, C. Xiang, S. Haussener, A.D. Bergercd and N.S. Lewis. Energy Environ. Sci., 6, 2984 (2013).
9. M. Lublow, S. Kubala, J.-F. Veyan and Y. J. Chabal. J. Applied Physics., 111, 084302 (2012).
10. R. Fan, Z.Mi, M.Shen. Optics Express, 27, A51 (2019).
11. S. Sarnchez de la Morena, G. Recio-Sarnchez, V. Torres-Costa and R.J. Martırn-Palma. Scripta Materialia 74, 33 (2014).
12. H. Hana, Z. Huang, W. Lee. Nano Today., 9, 271 (2014)
13. W. Vijselaar, R. M. Tiggelaar, H. Gardeniers, J. Huskens. ACS Energy Lett., 3, 1086 (2018).
14. J. Salonen and E. Mäkilä. Adv. Mater., 30, 1 (2018).
15. K. Tynyshtykbayev, Ch. Spitas, K. Kostas, Z. Insepov. ECS J. Solid State Sci.Tech., 10, 013009 (2021).
16. K. B. Tynyshtykbaev, T. Aitmukan, A. T. Issova, B. A. Rakhymetov, M.A. Yeleuov, and S. Z. Tokmoldin. Materials Sciences and Applications, 4, 1 (2013).
17. I. H. Campbell, P.M. Fauchet. Solid State Communications., 58, 739(1986).
18. V. I. Kukushkin, V. E. Kirpichev, E. N. Morozova, V. V Solovyev, Y. V. Fedotova, I. V. Kukushkin. JETP Letters., 112 , 31 (2020).
19. D. W. Boukhvalov, D.A. Zatsepin, D. Yu. Biryukov, Yu.V. Shchapova, N.V. Gavrilov, A.F. Zatsepin. Appl. Surf. Sci., 666, 160379 (2024).
20. A. R. Neale, Y. Jin, J. Ouyang, S. Hughes, D. Hesp, V. Dhanak, G. Dearden, S. Edwardson, L.J. Hardwick. J. Power Sources., 271, 42 (2014).
21. N. Yarykin, J. Weber. Appl. Phys. Lett., 109, 102101 (2016).
22. D. W. Boukhvalov, B. Zhumabay, P. Kusherova, B. Rakymetov, K. B. Tynyshtykbayev, A. S. Serikkanov and N. V. Chuchvaga. RSC Adv., 15, 6794 (2025).
23. D. W. Boukhvalov, K. A. Abdullin, T. S. Turmagambetov, A. K. Shongalova, I. S. Nevmerzhitskiy, A.S. Serikkanov. Sep. Pur. Tech., 334 126107 (2024).
24. M. Kanamori, H. Tsuya. Jpn. J. Appl. Phys. 24 557 (1985).
25. L. Bokobza, J.-L. Bruneel and M. Couzi. J. Carbon Res. 1 , 77 (2015).